



# *Eigenvalue calculator for Islanded Inverter-Based Microgrids*

A. Mahmoudi<sup>1</sup>, S. H. Hosseinian<sup>2\*</sup> and M. Kosari<sup>1</sup>

1-PhD. Student, Electrical Engineering Department, Amirkabir University of Technology, Tehran, Iran.

2- Professor, Department of Electrical Engineering, Amirkabir University of Technology, Tehran, Iran.

## **ABSTRACT**

The stability analysis of islanded inverter-based microgrids (IBMGs) is increasingly an important and challenging topic due to the nonlinearity of IBMGs. In this paper, a new linear model for such microgrids as well as an iterative method to correct the linear model is proposed. Using the linear model makes it easy to analyze the eigenvalues and stability of IBMGs due to the fact that it derives the eigenvalues directly and the linearization around an operating point to study the small signal stability and also use the newton-raphson method or other load flow solutions to solve these systems are no longer needed. An effective eigenvalue calculator is developed which is able to calculate the eigenvalues of IBMGs in the first few iterations of the proposed method. The proposed method provides the superior performance considering the simulation time compared to the conventional methods. The validation and comparison of the results show the performance of the proposed method.

## **KEYWORDS**

Inverter-based microgrids, Stability analysis, Eigenvalue calculator, Linear models, State-space model.

\*

Corresponding Author, Email: hosseinian@aut.ac.ir

## 1- INTRODUCTION

The development of the distributed generation (DG) in distribution networks was the introduction of microgrids (MGs) [1]. Although standards [2-3] prohibit active voltage regulation and islanded operation of MGs, the high penetration of DG units and power system outage necessitate controlling the provisions for both grid-connected and autonomous operation mode of MG units. Highly reliable electric supply service and good power quality for customers are the main advantages of islanded MGs when the utility is unavailable [4]. Due to the relatively small size of MGs, the system frequency and voltage regulation are dictated by the main network in grid-connected mode. However, in the islanded mode of operation, their regulation is a critical control task and is dictated only by DGs. A communication link or a droop method is used in the literature to fulfill this objective. A dispatch signal is used to control DG outputs when a master-slave link is involved in communication approaches [5-6]. In conventional power systems, frequency/real power and voltage/reactive power droop control have extensively been used. Based on this concept, in the literature, several droop control schemes have been suggested for the islanded operation of MGs [7-13].

The main advantage of the droop control methods is that a communication link is no longer needed and MGs can be supported by any of DGs irrespective of which sources are available. Conventional droop control methods have a good performance for inductive lines but their performance is poor for the resistive lines. To solve this issue and also to improve the droop controller, several strategies have been proposed including the droop parameter adjustment, use of proportional, integral, and derivative controllers within the droop calculation [14-20].

Large and small disturbance studies in MGs are entitled 'the transient stability' and 'the small-signal stability'. Time-variant power outputs in renewable sources can be regarded as small disturbances and it can also be coupled with load fluctuations [21]. The operation status of MGs can be affected by these kinds of small power fluctuations and it necessitates studying small-signal stability which has been studied in the literature frequently [7-11], [21-23]. However, the transient stability of MGs has been studied rarely [24-25] due to that the nonlinear properties of such systems make analytical tools particularly cumbersome and only a time-series simulation technique provides sufficient fidelity for examining that [26].

In this paper, a new linear model for islanded IBMGs is proposed. An iterative method is proposed to correct the linear model and perform a dynamic simulation. The proposed method can deal with the mentioned difficulties and challenges and makes it easy to simulate and analyze IBMGs. The eigenvalues of such MGs are calculated very fast and easy due to the fact that load-flow solutions to obtain a steady-state operating point are no longer needed. Indeed, the eigenvalues of IBMGs are calculated in the first few iterations of the proposed method using an effective eigenvalue calculator. The stability of IBMGs according to line impedances and other system parameters can be easily studied using the eigenvalue calculator. The iterative method dynamically corrects the state matrix as well as eigenvalues when a fault is occurred. The proposed method provides superior performance considering the simulation time compared to the conventional methods.

This paper will cover three main parts: The linear time-invariant (LTI) state-space model for IBMGs is proposed in the first part. To correct the linear model and perform a dynamic simulation, an iterative method is developed in the second part. The proposed method is verified in the third part.

## 2- PROPOSED LTI STATE-SPACE MODEL

The most general state-space representation of a linear system can be written in the following form:

$$\dot{x}(t) = A(t)x(t) + B(t)u(t) \quad y(t) = C(t)x(t) + D(t)u(t) \quad (1)$$

An LTI form of (1) can be written as:

$$\dot{x}(t) = Ax(t) + Bu(t) \quad y(t) = Cx(t) + Du(t) \quad (2)$$

where  $A$ ,  $B$ ,  $C$  and  $D$  are the constant matrices. The state vector of the LTI system is obtained as:

$$x(t) = e^{At}x(0) + \int_0^t e^{A(t-\tau)}Bu(\tau)d\tau \quad (3)$$

The stability of the system can also be studied using the eigenvalues of  $A$ . These useful characteristics can be used to study IBMGs, although they have nonlinear properties. Fortunately, the nonlinear properties are sparse and restricted to the multiplication of variables as can be seen in the next section. This paper tries to extract a linear model for IBMGs to achieve those advantages. To develop a step-by-step LTI model, each subsystem of IBMGs is modified and its corresponding LTI model is presented as follows:

## A. INVERTER MODEL

An inverter of a DG and its subsystems are shown in Fig. 1.

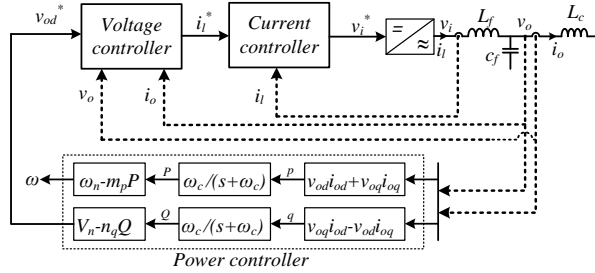


Fig. 1. A simple diagram of an inverter

1) *Power controller*: as can be seen in Fig. 1, instantaneous power components of an inverter, i.e.  $p$  and  $q$ , are calculated as:

$$p = v_{od} i_{od} + v_{oq} i_{oq} \quad q = v_{oq} i_{od} - v_{od} i_{oq} \quad (4)$$

The real and reactive powers of the inverter are obtained by passing the instantaneous powers through a low-pass filter as:

$$\begin{aligned} P &= \omega_c / (s + \omega_c) p & Q &= \omega_c / (s + \omega_c) q \\ \dot{P} &= \omega_c (v_{od} i_{od} + v_{oq} i_{oq} - P) & \dot{Q} &= \omega_c (v_{oq} i_{od} - v_{od} i_{oq} - Q) \end{aligned} \quad (5)$$

where  $\omega_c$  is the cut-off frequency of the low-pass filter. It is obvious that, in power systems, small changes in voltages around nominal values are observed. Therefore, (5) can be linearized as:

$$\dot{P} = \omega_c (v_{od}^{(0)} i_{od} + v_{oq}^{(0)} i_{oq} - P) \quad \dot{Q} = \omega_c (v_{oq}^{(0)} i_{od} - v_{od}^{(0)} i_{oq} - Q) \quad (6)$$

where  $v_{od}^{(0)}$  and  $v_{oq}^{(0)}$  are the nominal voltages of  $d$  and  $q$  axes or other initial values. The angle between an individual inverter reference frame and the common reference frame,  $\delta$ , can be obtained as:

$$\begin{aligned} \dot{\delta} &= \omega - \omega_{com} & \omega &= \omega_n - m_p P \\ \dot{\delta} &= m_{pcom} P_{com} - m_p P \end{aligned} \quad (7)$$

where  $m_p$  is the active power droop gain and the subscript "com" denotes the variables of an inverter, the reference frame of which is taken as the common reference frame.

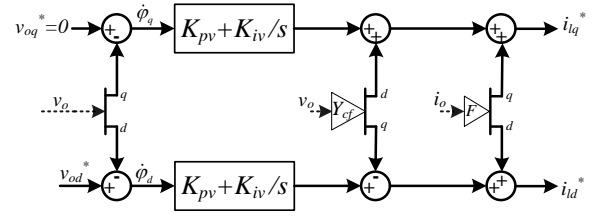


Fig. 2. Voltage controller of an inverter  $Y_{cf} = \omega_n C_f$  and  $F$  is a constant value

1) *Voltage controller*: as can be seen in Fig. 2, state variables in this section are the differences between the reference and feedback voltages and can be written as:

$$\dot{\phi}_d = v_{od}^* - v_{od} \quad \dot{\phi}_q = v_{oq}^* - v_{oq} \quad (8)$$

Using the conventional droop control method, (8) can be rewritten as:

$$\dot{\phi}_d = V_n - n_q Q - v_{od} \quad \dot{\phi}_q = -v_{oq} \quad (9)$$

where  $n_q$  is the reactive power droop gain. It should be noted that the conventional droop control is used only for the sake of simplicity.

1) *Current controller*: as shown in Fig. 3, the state equations of this section can be written as:

$$\dot{\gamma}_d = i_{ld}^* - i_{ld} \quad \dot{\gamma}_q = i_{lq}^* - i_{lq} \quad (10)$$

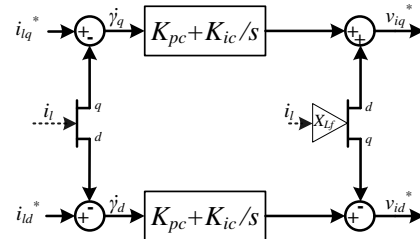


Fig. 3. Current controller of an inverter  $X_{Lf} = \omega_n L_f$

Substituting the reference currents,  $i_{ld}^*$  and  $i_{lq}^*$ , calculated in the voltage controller, and after some manipulation, (10) can be rewritten as:

$$\begin{aligned} \dot{\gamma}_d &= F i_{od} - \omega_n C_f v_{oq} + K_{pv} (V_n - n_q Q - v_{od}) + K_{iv} \phi_d - i_{ld} \\ \dot{\gamma}_q &= F i_{oq} + \omega_n C_f v_{od} - K_{pv} v_{oq} + K_{iv} \phi_q - i_{lq} \end{aligned} \quad (11)$$

The LTI state-space model of the controllers can be written as:

$$\dot{x}_1 = A_1 x + B_1 u + C_1 P_{com} \quad (12)$$

where

$$x_1 = [P \quad Q \quad \varphi_d \quad \varphi_q \quad \gamma_d \quad \gamma_q \quad \delta]^T$$

$$x_2 = [i_{ld} \quad i_{lq} \quad v_{od} \quad v_{oq} \quad i_{od} \quad i_{oq}]^T$$

$$x = [x_1 \quad x_2]^T \quad u = [V_n \quad \omega_n]^T$$

$$A_1 = \begin{bmatrix} -\omega_c a_1 & 0 & 0_{2 \times 3} & 0 & 0 & \omega_c a_2 \\ a_3 & 0 & 0 & 0 & -a_1 & 0 \\ K_{pv} a_3 & K_{iv} a_1 & 0 & -a_1 & a_4 & F a_1 \\ a_5 & 0 & 0 & 0 & 0 & 0 \end{bmatrix}_{7 \times 13}$$

$$B_1 = \begin{bmatrix} 0 & 0 & 1 & 0 & K_{pv} & 0 & 0 \\ 0 & 0 & 0 & 0 & 0 & 0 & 0 \end{bmatrix}^T \quad C_1 = [0_{1 \times 6} \quad m_{pcom}]^T$$

$$a_1 = \begin{bmatrix} 1 & 0 \\ 0 & 1 \end{bmatrix} \quad a_2 = \begin{bmatrix} v_{od}^{(0)} & v_{oq}^{(0)} \\ v_{oq}^{(0)} & -v_{od}^{(0)} \end{bmatrix} \quad a_3 = \begin{bmatrix} 0 & -n_q \\ 0 & 0 \end{bmatrix}$$

$$a_4 = \begin{bmatrix} -K_{pv} & -\omega_n C_f \\ \omega_n C_f & -K_{pv} \end{bmatrix} \quad a_5 = [-m_p \quad 0]$$

As can be seen in (12), the nominal voltage and frequency are the inputs of the system and can affect the steady-state operating point of IBMGs.

2) *Output LC filter and coupling Inductance*: if the inverter produces the demanded voltage ( $v_i = v_i^*$ ), the linearized state space model of this section in similar manner is given by (13).

$$\begin{aligned} \dot{i}_{ld} &= (\omega^{(0)} L_f i_{lq} - r_f i_{ld} + v_{id} - v_{od}) / L_f \\ \dot{i}_{lq} &= (-\omega^{(0)} L_f i_{ld} - r_f i_{lq} + v_{iq} - v_{oq}) / L_f \\ \dot{v}_{od} &= (\omega^{(0)} C_f v_{oq} + i_{ld} - i_{od}) / C_f \\ \dot{v}_{oq} &= (-\omega^{(0)} C_f v_{od} + i_{lq} - i_{oq}) / C_f \\ \dot{i}_{od} &= (-r_c i_{od} + \omega^{(0)} L_c i_{oq} + v_{od} - v_{bd}) / L_c \\ \dot{i}_{oq} &= (-r_c i_{oq} - \omega^{(0)} L_c i_{od} + v_{oq} - v_{bq}) / L_c \end{aligned} \quad (13)$$

The linearized form is based on the fact that the frequency drop of IBMGs is very slight and  $\omega$  is very close to  $\omega_n$ , therefore,  $\omega^{(0)}$  can be assumed to be  $\omega_n$  or an initial condition. The first two equations of (13) contain  $v_i$  which isn't a state variable so it must be replaced. These equations can be rewritten as:

$$\begin{aligned} \dot{i}_{ld} &= (-k_1 n_q Q + k_2 \varphi_d + K_{ic} \gamma_d - (K_{pc} + r_f) i_{ld} - (1 + k_1) v_{od} \\ &\quad - \omega_n C_f K_{pc} v_{oq} + F K_{pc} i_{od} - K_{pc} \Delta \omega^{(0)} i_{lq} + k_1 V_n) / L_f; \end{aligned} \quad (14)$$

$$\begin{aligned} \dot{i}_{lq} &= (k_2 \varphi_q + K_{ic} \gamma_q - (K_{pc} + r_f) i_{lq} + \omega_n C_f K_{pc} v_{od} \\ &\quad - (1 + k_1) v_{oq} + F K_{pc} i_{od} + K_{pc} \Delta \omega^{(0)} i_{ld}) / L_f; \end{aligned}$$

$$k_1 = K_{pc} K_{pv} \quad k_2 = K_{pc} K_{iv} \quad \Delta \omega^{(0)} = \omega_n - \omega^{(0)}$$

The corresponding LTI state-space model for this filter and coupling inductance can be obtained as:

$$\dot{x}_2 = A_2 x + B_2 u + C_2 v_{bdq} \quad (15)$$

where

$$A_2 = \frac{1}{L_f} \begin{bmatrix} k_1 a_3 & k_2 a_1 & K_{ic} a_1 & 0_{2 \times 1} & a_6 & a_7 & K_{pc} F a_1 \\ 0 & 0 & 0 & 0 & k_3 a_1 & a_8 & -k_3 a_1 \\ 0 & 0 & 0 & 0 & 0 & k_4 a_1 & a_9 \end{bmatrix}_{6 \times 13}$$

$$a_6 = \begin{bmatrix} -r_f - K_{pc} & -\Delta \omega^{(0)} L_f \\ \Delta \omega^{(0)} L_f & -r_f - K_{pc} \end{bmatrix} \quad a_7 = \begin{bmatrix} -1 - k_1 & -K_{pc} \omega_n C_f \\ K_{pc} \omega_n C_f & -1 - k_1 \end{bmatrix}$$

$$a_8 = L_f \begin{bmatrix} 0 & \omega^{(0)} \\ -\omega^{(0)} & 0 \end{bmatrix} \quad a_9 = k_4 \begin{bmatrix} -r_c & \omega^{(0)} L_c \\ -\omega^{(0)} L_c & -r_c \end{bmatrix}$$

$$B_2 = \frac{1}{L_f} \begin{bmatrix} k_1 & 0_{1 \times 5} \\ 0 & 0 \end{bmatrix}^T \quad C_2 = \begin{bmatrix} 0_{2 \times 4} & \frac{-1}{L_c} a_1 \end{bmatrix}^T$$

$$v_{bdq} = \begin{bmatrix} v_{bd} \\ v_{bq} \end{bmatrix} \quad k_3 = \frac{L_f}{C_f} \quad k_4 = \frac{L_f}{L_c}$$

3) *Inverter connections*: The output currents of an individual inverter,  $i_{odq}$ , must be converted to the common reference frame to connect the inverter to the whole system. These currents on the common reference frame are represented by  $i_{oDQ}$  and can be given by:

$$\begin{bmatrix} i_{oD} \\ i_{oQ} \end{bmatrix} = T \begin{bmatrix} i_{od} \\ i_{oq} \end{bmatrix} \quad \text{where } T = \begin{bmatrix} \cos \delta & -\sin \delta \\ \sin \delta & \cos \delta \end{bmatrix} \quad (16)$$

Moreover, the bus voltage is the input signal of the inverter and must be converted from the common reference frame to an individual inverter reference frame as:

$$v_{bdq} = T^{-1} v_{bDQ} \quad \text{where } v_{bDQ} = [v_{bD} \quad v_{bQ}]^T \quad (17)$$

When different loads or network impedances force inverters to work in different frames, the effect of  $\delta$  on the stability of IBMGs is important, thus it must be considered as a main state variable in the linearization. On the other hand,  $\delta$  is small and around zero (i.e.  $\cos \delta \approx$

1 and  $\sin\delta \approx \delta$ ). Hence, (16) and (17) are linearized based on these facts as:

$$\begin{aligned} i_{oD} &= i_{od} - i_{oq}^{(0)} \delta & i_{oQ} &= i_{oq} + i_{od}^{(0)} \delta \\ v_{bD} &= v_{bD} + v_{bQ}^{(0)} \delta & v_{bQ} &= v_{bQ} - v_{bD}^{(0)} \delta \end{aligned} \quad (18)$$

where  $i_{od}^{(0)}$ ,  $i_{oq}^{(0)}$ ,  $v_{bD}^{(0)}$  and  $v_{bQ}^{(0)}$  can be the nominal values or other initial values.

A complete LTI state-space model of inverter  $i$  can be obtained by combining (12), (15) and (18) as:

$$\begin{aligned} \dot{x}_{INVi} &= A_{INVi} x_{INVi} + B_{INVi} u + C_{INVi} [P_{com} v_{bDQi}]^T \\ i_{oDQi} &= D_{INVi} x_{INVi} \end{aligned} \quad (19)$$

where

$$\begin{aligned} x_{INVi} &= x \quad A_{INVi} = [A_1 \quad A_2]^T + A_\delta \quad B_{INVi} = [B_1 \quad B_2]^T \\ D_{INVi} &= \begin{bmatrix} 0_{1 \times 6} & -i_{oq}^{(0)} & 0_{1 \times 4} & 1 & 0 \\ 0 & i_{od}^{(0)} & 0 & 0 & 1 \end{bmatrix}_{2 \times 13} \quad C_{comi} = \begin{bmatrix} C_1 \\ 0 \end{bmatrix} \quad C_{DQi} = \begin{bmatrix} 0 \\ C_2 \end{bmatrix} \\ A_\delta &= \frac{1}{L_c} \begin{bmatrix} 0_{11 \times 6} & 0 & 0_{11 \times 6} \\ 0 & -v_{bQ}^{(0)} & 0 \\ 0 & v_{bD}^{(0)} & 0 \end{bmatrix}_{13 \times 13} \quad C_{INVi} = \begin{bmatrix} C_{comi} & C_{DQi} \end{bmatrix} \end{aligned}$$

6) *Combined model of Inverters*: if there is a MG with  $n_i$  inverter-based DGs, the reference frame of DG 1 is taken as the common reference frame, i.e.  $\omega_1$  assigned as  $\omega_{com}$ , and it is the reference frequency signal for other inverters, network and loads. Reactances of the network and loads and also  $\delta$  is calculated based on this frequency. By combining the models of all inverters, a combined LTI state-space model is obtained as:

$$\begin{aligned} \dot{x}_{INV} &= A_{INV} x_{INV} + B_{INV} u + C_{INV} v_{bDQ} \\ i_{oDQ} &= D_{INV} x_{INV} \end{aligned} \quad (20)$$

Where

$$\begin{aligned} A_{INV} &= \begin{bmatrix} A_{INV1} + C_{com1} & 0 & \cdots & 0 \\ C_{com2} & A_{INV2} & \cdots & 0 \\ \vdots & \vdots & \ddots & \vdots \\ C_{comn_i} & 0 & \cdots & A_{INVn_i} \end{bmatrix}_{13n_i \times 13n_i} \\ B_{INV} &= \begin{bmatrix} B_{INV1} \\ B_{INV2} \\ \vdots \\ B_{INVn_i} \end{bmatrix}_{13n_i \times 2} \quad v_{bDQ} = \begin{bmatrix} v_{bDQ1} \\ v_{bDQ2} \\ \vdots \\ v_{bDQn_b} \end{bmatrix} \quad x_{INV} = \begin{bmatrix} x_{INV1} \\ x_{INV2} \\ \vdots \\ x_{INVn_i} \end{bmatrix} \end{aligned}$$

$$\begin{aligned} C_{INV} &= \begin{bmatrix} C_{DQ1} & 0 & \cdots & 0 & \cdots & 0 \\ 0 & C_{DQ2} & \cdots & 0 & \cdots & 0 \\ \vdots & \vdots & \ddots & \vdots & \ddots & \vdots \\ 0 & 0 & \cdots & C_{DQn_i} & \cdots & 0 \end{bmatrix}_{13n_i \times 2n_b} \\ D_{INV} &= \begin{bmatrix} D_{INV1} & 0 & \cdots & 0 \\ 0 & D_{INV2} & \cdots & 0 \\ \vdots & \vdots & \ddots & \vdots \\ 0 & 0 & \cdots & D_{INVn_i} \end{bmatrix}_{2n_i \times 13n_i} \quad i_{oDQ} = \begin{bmatrix} i_{oDQ1} \\ i_{oDQ2} \\ \vdots \\ i_{oDQn_i} \end{bmatrix} \end{aligned}$$

It should be noted that  $n_b$  is the number of network buses and it may be greater than  $n_i$  i.e.  $n_i \leq n_b$ .

## B. LINE AND LOAD MODELS

In a similar manner, the linearized state equations of line  $i$  connecting bus  $j$  to  $k$ , are given by:

$$\begin{aligned} \dot{i}_{lineDi} &= (-r_{linei} i_{lineDi} + \omega_1^{(0)} L_{linei} i_{lineQi} + v_{bDj} - v_{bDk}) / L_{linei} \\ \dot{i}_{lineQi} &= (-r_{linei} i_{lineQi} - \omega_1^{(0)} L_{linei} i_{lineDi} + v_{bQj} - v_{bQk}) / L_{linei} \end{aligned} \quad (21)$$

If there are  $n_n$  lines, then the LTI state-space model of this network can be written as:

$$\dot{i}_{lineDQ} = A_{NET} i_{lineDQ} + C_{NET} v_{bDQ} \quad (22)$$

where

$$\begin{aligned} A_{NET} &= \frac{1}{L_{linei}} \begin{bmatrix} A_{NET1} & 0 & \cdots & 0 \\ 0 & A_{NET2} & \cdots & 0 \\ \vdots & \vdots & \ddots & \vdots \\ 0 & 0 & \cdots & A_{NETn_n} \end{bmatrix}_{2n_n \times 2n_n} \\ i_{lineDQ} &= \begin{bmatrix} i_{lineDQ1} \\ i_{lineDQ2} \\ \vdots \\ i_{lineDQn_n} \end{bmatrix} \quad C_{NET} = \begin{bmatrix} C_{NET1} \\ C_{NET2} \\ \vdots \\ C_{NETn_n} \end{bmatrix}_{2n_n \times 2n_b} \\ A_{NETi} &= \begin{bmatrix} -r_{linei} & \omega_1^{(0)} \\ -\omega_1^{(0)} & -r_{linei} \end{bmatrix} \quad C_{NETi} = \frac{1}{L_{linei}} \begin{bmatrix} \cdots & 1 & 0 & \cdots & -1 & 0 & \cdots \\ \cdots & 0 & 1 & \cdots & 0 & -1 & \cdots \end{bmatrix}_{2 \times 2n_b} \end{aligned}$$

the linearized state equations of a general  $RL$  load can be given for the load connected at  $j$ -th bus as:

$$\begin{aligned} \dot{i}_{loadDj} &= (-R_{loadj} i_{loadDj} + \omega_1^{(0)} L_{loadj} i_{loadQj} + v_{bDj}) / L_{loadj} \\ \dot{i}_{loadQj} &= (-R_{loadj} i_{loadQj} - \omega_1^{(0)} L_{loadj} i_{loadDj} + v_{bQj}) / L_{loadj} \end{aligned} \quad (23)$$

If there are  $n_l$  loads, then the LTI state-space model of the loads is given by:

$$\dot{i}_{loadDQ} = A_{LOAD} i_{loadDQ} + C_{LOAD} v_{bDQ} \quad (24)$$

where

$$A_{LOAD} = \frac{1}{L_{loadi}} \begin{bmatrix} A_{LOAD1} & 0 & \dots & 0 \\ 0 & A_{LOAD2} & \dots & 0 \\ \vdots & \vdots & \ddots & \vdots \\ 0 & 0 & \dots & A_{LOADn_i} \end{bmatrix}_{2n_i \times 2n_i}$$

$$i_{loadDQ} = \begin{bmatrix} i_{loadDQ1} \\ i_{loadDQ2} \\ \vdots \\ i_{loadDQn_i} \end{bmatrix} \quad C_{LOAD} = \frac{1}{L_{loadi}} \begin{bmatrix} C_{LOAD1} \\ C_{LOAD2} \\ \vdots \\ C_{LOADn_i} \end{bmatrix}_{2n_i \times 2n_b}$$

$$A_{LOADi} = \begin{bmatrix} -R_{loadi} & \omega_1^{(0)} \\ -\omega_1^{(0)} & -R_{loadi} \end{bmatrix} \quad C_{LOADi} = \begin{bmatrix} \dots & 1 & 0 & \dots \\ \dots & 0 & 1 & \dots \end{bmatrix}_{2 \times 2n_b}$$

### C. COMPLETE MG MODEL

If each bus is connected to ground with a large resistor,  $r_g$ , bus voltages can be expressed based on the current of this resistor as:

$$v_{bDQ} = R_G (M_{INV} i_{oDQ} - M_{load} i_{loadDQ} - M_{NET} i_{lineDQ}) \quad (25)$$

where  $R_G$  is a  $2n_b \times 2n_b$  diagonal matrix and all the diagonal entries are  $r_g$ .  $M_{INV}$ ,  $M_{load}$  and  $M_{NET}$  show the links among inverters, loads and lines with network buses, respectively. By applying a simple KCL in bus  $i$ , the elements of row  $i$  of these matrixes can be easily specified. The resistance of  $r_g$  is selected sufficiently large to minimum the influence of its introduction.

Consequently, the complete LTI state-space model of IBMGs can be obtained through combining the LTI state-space model of the individual subsystems given by (20), (22), (24) and (25) as:

$$\dot{X} = A_{sys} X + B_{sys} u \quad (26)$$

where

$$A_{sys} = \begin{bmatrix} A_{INV} + C_{INV} R_N M_{INV} D_{INV} & -C_{INV} R_N M_{NET} & -C_{INV} R_N M_{load} \\ C_{NET} R_N M_{INV} D_{INV} & A_{NET} - C_{NET} R_N M_{NET} & -C_{NET} R_N M_{load} \\ C_{LOAD} R_N M_{INV} D_{INV} & -C_{LOAD} R_N M_{NET} & A_{LOAD} - C_{LOAD} R_N M_{load} \end{bmatrix}$$

$$B_{sys} = \begin{bmatrix} B_{INV} \\ 0 \\ 0 \end{bmatrix} \quad X = \begin{bmatrix} x_{INV} \\ i_{lineDQ} \\ i_{loadDQ} \end{bmatrix}$$

### 3- PROPOSED ITERATIVE METHOD

A few variables were replaced with constant values notated using superscript (0) in the previous section to linearize some equations and to form the system matrix,  $A_{sys}$ . To improve the accuracy and also to perform a dynamic simulation, these variables are updated using an iterative method.

It should be noted that  $B_{sys}$  is constant and there is no

need to update it. It is required to update only 4 elements when an individual inverter reference frame is converted into the common reference frame, and vice versa. The number of elements, which must be updated for each inverter, line and load, is shown in Table 1. On the other hand, as can be seen in (29), for the line and load model, only  $\omega_l$  must be updated and it is obvious that a small drop in  $\omega_l$  compared to  $\omega_n$  is observed as will be seen in the tests results.

Fig. 4 shows a simple flowchart of the proposed iterative method. This iterative method can be used for two purposes:

#### 1) Quick calculation of eigenvalues (eigenvalue calculator)

the iterative method can calculate eigenvalues in the first few iterations even if the system steady-state is not reached. Indeed, eigenvalues are independent of the steady-state operating point and when variations of  $X$  are limited to a normal range, the modes of the system can be calculated from  $A_{sys}$  with a reasonable accuracy. This advantage of the proposed method can be used as a good alternative tool to quickly evaluate the stability of IBMGs. As shown in Fig. 4, an error tolerance for eigenvalues,  $\varepsilon_A$ , is defined to ensure that eigenvalues is calculated with a reasonable accuracy.

#### 2) Performing a dynamic simulation

the proposed method can also perform a complete dynamic simulation which drives the transient response of IBMGs as well as a steady-state operating point. Eigenvalues are calculated in each iteration and when the steady-state is reached, the final values of them are derived. To ensure that the system steady-state is reached, an error tolerance for the state vector,  $\varepsilon_X$ , is defined.

### 4- TEST RESULTS

A 220 V (per phase RMS), 50 Hz prototype MG shown in Fig. 5 is studied. A resistive load of 5.8 kW (25Ω per phase), 4.8 kW (30 Ω per phase) and 7.3 kW (20 Ω per phase) at buses 1, 2 and 3 are considered, respectively. The parameters of the inverters (with the same ratings, 10 kVA) are the same as those given in Table 2, except the active power droop gains

TABLE 1. The number of elements which must be updated at each iteration

Items	Inverter	Line	Load
Number of items	$n_i$	$n_n$	$n_l$
Number of updated elements	$10n_i + 4(n_i - 1)$	$2n_n$	$2n_l$

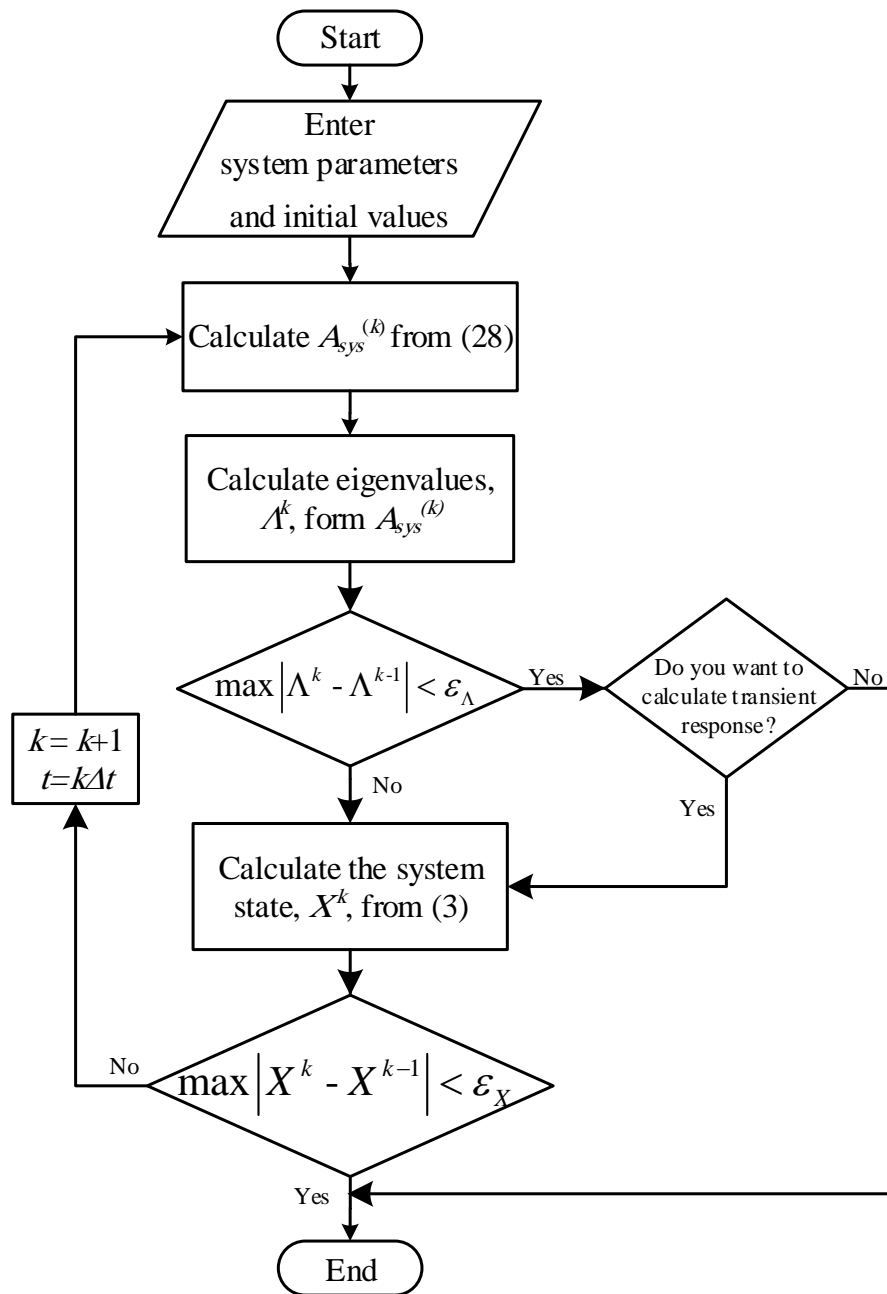


Fig. 4. A simple flowchart of the proposed iterative method

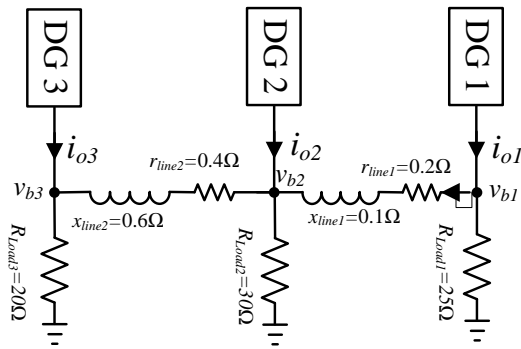


Fig. 5. Test system

TABLE 2. INVERTER PARAMETERS OF THE TEST SYSTEM

Par.	Value	Par.	Value	Par.	Value
$f_s$	8 kHz	$r_{Lc}$	0.03 Ω	$K_{iv}$	390
$L_f$	1.35 mH	$\omega_c$	31.41	$K_{pc}$	10.5
$C_f$	50 μF	$m_p$	9.4e-5	$K_{ic}$	16e3
$r_f$	0.1 Ω	$n_q$	1.3e-3	$F$	0.75
$L_c$	0.35 mH	$K_{pv}$	0.05		

which different and the same values for them are used in the following tests. It should be noted that in this paper, only  $m_p$  is varied and the reactive power droop gain,  $n_q$ , is constant so the droop gain in the paper refers to  $m_p$ . To verify the proposed method, three tests are presented as follows:

**Test 1: a small-signal test:** in this test, the real power of Load 1,  $P_{Load1}$ , is switched to 11.6 Kw (12.5Ω per phase) i.e. it becomes twice. The real power response of DGs is shown in Figs. 6 and 7 when different and the same droop gains are used. The transient time in Fig. 6 is about 150 ms whereas it is about 250 ms in Fig. 7 which means different droop gains improve the system stability. The changed load is close to DG1 and also the droop gain of Inverter 1,  $m_p(1)$ , is selected smaller than others which makes it possible for DG1 to participate actively in feeding increased amount of Load 1 whereas the other two DGs have limited participation in this test. The power flows of the lines are limited using different droop gains so the bus voltage and frequency variations are limited and the steady-state is reached quickly.

In Fig. 7, using the same droop gains make the inverters to share increased amount of  $P_{Load1}$  equally. As a result, the power flows of the lines as well as the variations of the bus voltages increase and thus the steady-state is reached slowly. DG1 takes the major part

of the transient because the variation of  $V_{b1}$  is caused by the power changes of the three DGs whereas the variations of  $V_{b2}$  and  $V_{b3}$  are affected by the power changes of the last two DGs and only DG3, respectively.

Table 3 shows the effective eigenvalues of the test system in Test 1 using the proposed method and the approach proposed by [10]. The results of the proposed method consist of steady-state or final values and those obtained from the eigenvalue calculator. As discussed, the results show that the system stability improves using different droop gains and also it shows that the proposed method has reasonable accuracy as compared with the method suggested by [10]. Consequently, showing the same performance in Figs. 6 and 7 and also Table 3 ensures the accuracy of the proposed method.

In Fig. 8, the influence of the line impedances on the system stability are studied. The initial values of the line impedances are gradually increased up to the point where the stability is no longer attained. The real part of the most effective eigenvalue, when the line impedances are varied by factor  $\alpha$ , is drawn in this figure. It is obvious that the system stability becomes worse as the line impedances increase and the figure shows the nonlinear decline of the stability as the line impedances increase. It also shows that small values for the line impedances make the system stability worse because inverters act as voltage sources and they must not be connected directly or with minor impedances.

**Test 2: a small-signal test:** in this test, the real power of Load 3,  $P_{load3}$ , is switched to 14.52 Kw (10 Ω per phase) i.e. it becomes twice. The reactive power response of the inverters is shown in Figs. 9 and 10 when different and the same droop gains are used, respectively. To balance bus voltages and compensate internal consumption in this case,  $Q_1$  decreases whereas  $Q_3$  increases. Increase in  $P_3$  could lead to the increase in the internal consumption of  $Q_3$ . Using reactive powers to balance bus voltages can be seen more clearly in Fig. 10 where the power flows of the lines increase



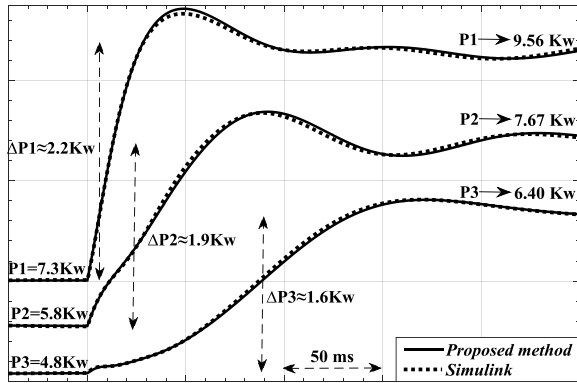


Fig. 6. Real power response of inverters when  $P_{Load1}$  is doubled and  $m_p = [8 \ 10 \ 12] \times 10^{-5}$ .

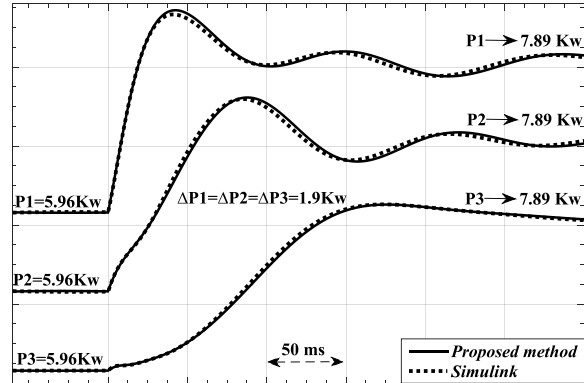


Fig. 7. Real power response of inverters when  $P_{Load1}$  is doubled and  $m_p(1:3) = 10e^{-5}$ .

TABLE 3. REAL PARTS OF EFFECTIVE EIGENVALUES WHEN  $P_{Load1}$  IS DOUBLED

Eff. Eig	The same droop gains $m_p(1:3) = 10e^{-5}$			different droop gains $m_p = [8 \ 10 \ 12] \times 10^{-5}$		
	Proposed method		Method by [10]	Proposed method		Method by [10]
	Final values	Eig. Calc.		Final values	Eig. Calc.	
$\lambda_9$	-80.912	-80.886	-80.478	-79.961	-79.940	-79.168
$\lambda_8$	-80.912	-80.886	-80.478	-79.961	-79.940	-79.168
$\lambda_7$	-52.253	-52.212	-52.207	-52.231	-52.192	-52.287
$\lambda_6$	-31.414	-31.414	-31.430	-31.414	-31.414	-31.440
$\lambda_5$	-31.410	-31.410	-31.395	-31.410	-31.410	-31.389
$\lambda_4$	-13.569	-13.592	-13.545	-13.376	-13.399	-13.307
$\lambda_3$	-13.569	-13.592	-13.545	-13.376	-13.399	-13.307
$\lambda_2$	-7.526	-7.535	-7.597	-8.499	-8.513	-8.548
$\lambda_1$	-7.526	-7.535	-7.597	-8.499	-8.513	-8.548

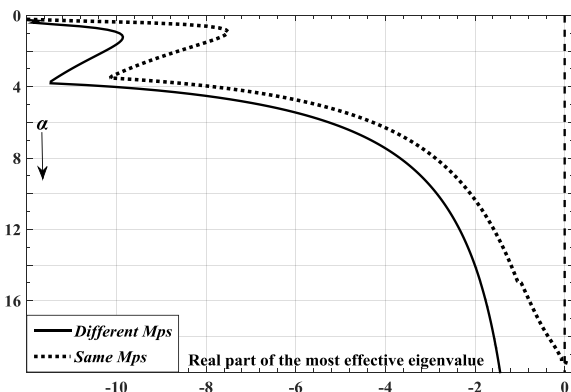


Fig. 8. The real part of the most effective eigenvalue as a function of  $\alpha$  when  $P_{Load1}$  is doubled and line impedances are varied by factor  $\alpha$ .

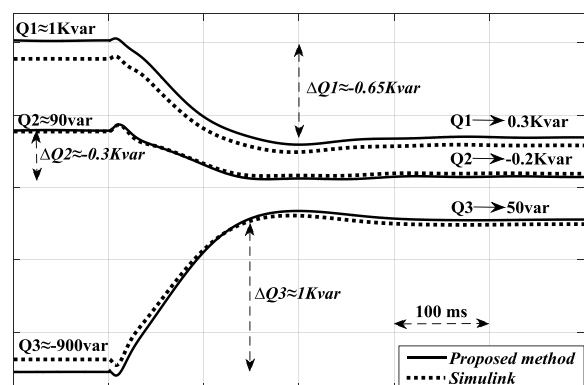


Fig. 9. Reactive power response of inverters when  $P_{Load3}$  is doubled and  $m_p = [15 \ 10 \ 5] \times 10^{-5}$ .

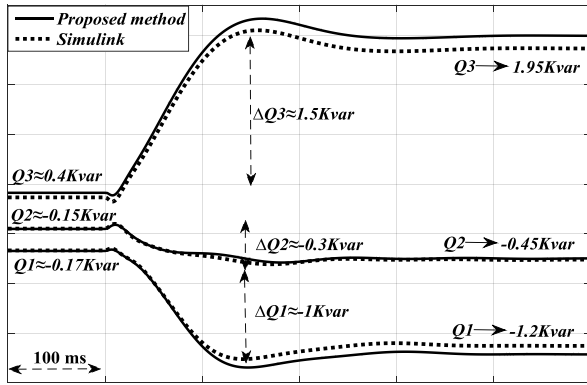


Fig. 10. Reactive power response of inverters when PLoad3 is doubled and  $m_p(1:3)=10e-5$ .

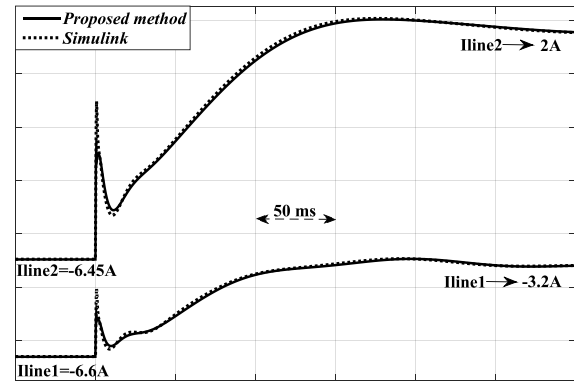


Fig. 11. Line currents (d-axis) response when  $P_3$  is doubled and  $m_p=[15 \ 10 \ 5] \times 1e-5$ .

TABLE 4. REAL PARTS OF THE EFFECTIVE EIGENVALUES WHEN  $P_{Load3}$  IS DOUBLED.

Eff. Eig	<i>The same droop gains <math>m_p(1:3)=10e-5</math></i>			<i>different droop gains <math>m_p=[15 \ 10 \ 5] \times 1e-5</math></i>		
	Proposed method		Method by [10]	Proposed method		Method by [10]
	Final values	Eig. Calc.		Final values	Eig. Calc.	
$\lambda_9$	-75.887	-75.987	-75.122	-77.327	-77.379	-77.391
$\lambda_8$	-75.887	-75.987	-75.122	-77.327	-77.379	-77.391
$\lambda_7$	-52.184	-52.233	-52.383	-52.159	-52.184	-52.166
$\lambda_6$	-31.419	-31.416	-31.458	-31.415	-31.416	-31.443
$\lambda_5$	-31.410	-31.410	-31.378	-31.410	-31.410	-31.388
$\lambda_4$	-13.637	-13.593	-13.499	-14.146	-14.129	-14.091
$\lambda_3$	-13.637	-13.593	-13.499	-14.146	-14.129	-14.091
$\lambda_2$	-7.524	-7.532	-7.544	-5.103	-5.124	-5.183
$\lambda_1$	-7.524	-7.532	-7.544	-5.103	-5.124	-5.183

TABLE 5. REAL PARTS OF THE EFFECTIVE EIGENVALUES WHEN DG3 IS DISCONNECTED

Eff. Eig	<i>The same droop gains <math>m_p=[10e-5 \ 10e-5]</math></i>				<i>different droop gains <math>m_p=[15e-5 \ 10e-5]</math></i>			
	Proposed method			[10]	Proposed method			[10]
	Bef. Fau.	Final values	Eig. Calc.		Bef. Fau.	Final values	Eig. Calc.	
$\lambda_9$	-81.00	-87.57	-87.59	-87.42	-83.40	-89.98	-89.98	-89.7
$\lambda_8$	-81.00	-87.57	-87.59	-87.42	-83.40	-89.98	-89.98	-89.7
$\lambda_7$	-52.16	--	--	--	-52.11	--	--	--
$\lambda_6$	-31.41	-31.42	-31.42	-31.44	-31.41	-31.42	-31.42	-31.4
$\lambda_5$	-31.41	-31.41	-31.41	-31.39	-31.41	-31.41	-31.41	-31.4
$\lambda_4$	-13.60	--	--	--	-14.13	--	--	--
$\lambda_3$	-13.60	--	--	--	-14.13	--	--	--
$\lambda_2$	-7.52	-6.92	-6.91	-6.98	-5.12	-4.47	-4.50	-4.53
$\lambda_1$	-7.52	-6.92	-6.91	-6.98	-5.12	-4.47	-4.50	-4.53

The effective eigenvalues of the test system when  $P_{Load3}$  is doubled are given in Table 4 using the proposed method and the method proposed by [10]. The results show that using different droop gains makes the stability of the system poor in this test. The droop gain of DG3 being closer to the changed load is selected smaller than others and better stability as Test 1 was expected. However, the large value of the impedance of Line 2 and overloading of DG3 causes such results.

Fig. 11 shows line current (d-axis) response when  $P_{Load3}$  is doubled and different droop gains are used. High-frequency oscillations can be seen in the line currents immediately after the switching action where the current of Line 2 reverses to participate in feeding  $P_{Load3}$  but it is small and not sufficient to prevent the overloading of DG3.

As can be seen in Figs. 9, 10, 11 and also Table 4, the proposed method also gives convincing results in this test.

**Test 3: a transient stability test:** in this test, DG3 is disconnected due to a fault and the other two DGs must supply loads. The active power response of the inverters is shown in Figs. 12 and 13 when different and the same droop gains are used, respectively. When different droop gains are used, there is a possibility to overload one of DGs as can be seen in Fig. 12 due to the heavy loadings. In Fig. 12, DG2 is closer to Load 3 and has a smaller droop gain so it participates actively in feeding Load 3 which leads to overloading of it while DG1 refuses to participate fully and equally. The transient response is also about 650 ms in case of different droop gains and 350 ms in the case of the same droop gains which show that the latter makes the system more stable.

The effective eigenvalues of the system in Test 3 are obtained through using the proposed method and the approach proposed by [10] in Table 5. In addition to the results of the eigenvalue calculator and the final values, the eigenvalues of the system before the fault are also given in the table. As discussed, the results show that the system stability improves using the same droop gains. However, the system stability becomes worse after the fault because of the heavy loadings in both two cases. As Table 5 shows, three effective eigenvalues are eliminated after the fault due to that DG3 as well as its eigenvalues are eliminated and the force on  $V_{b3}$  in a limited range around  $v_{o3}$  is also eliminated. Again, the figures and tables show reasonable accuracy for the proposed method compared to Simulink and the method suggested by [10].

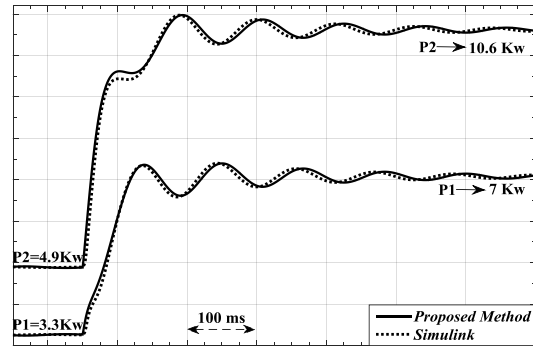


Fig. 12. Real power response of inverters when DG3 is disconnected and  $m_p=[15e-5 \ 10e-5]$ .

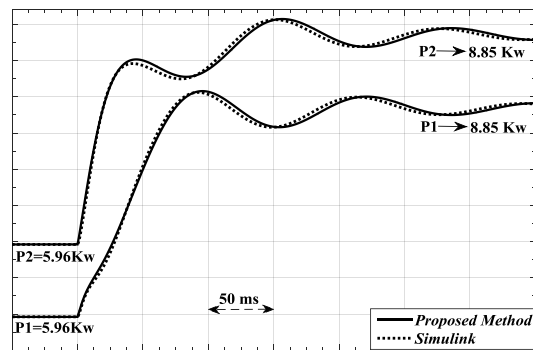


Fig. 13. Real power response of inverters when DG3 is disconnected and  $m_p=[10e-5 \ 10e-5]$ .

In Figs. 14 and 15, the system stability as a function of line impedances is studied in this test. When DG3 is disconnected, Line 2 can be assigned as a part of Load 3 and the influence of the resistance and reactance of Line 1 on the system stability can be investigated more clearly and separately. The real part of the most effective eigenvalue is plotted as a function of  $r_{line1}$  and  $x_{line1}$  when they are increased from zero to the point where the stability is no longer attained. In Fig. 14, this study is performed when the same droop gains are used and that is performed for different droop gains in Fig. 15.

The results show that, as expected, the resistance has more potential to threaten the system stability and this is the main disadvantage of the conventional droop control methods as discussed in the introduction. Increase in  $r_{line1}$  up to about 2.5  $\Omega$  improves the stability because it provides sufficient resistance to connect the two voltage sources. On the other hand, as  $r_{line1}$  increases more than 2.5  $\Omega$ , the most effective eigenvalue moves toward an unstable region making the system more oscillatory and eventually leading to instability when  $r_{line1}$  is over 9.6  $\Omega$  for the same droop gains and 17.5  $\Omega$  in the case of different droop gains.

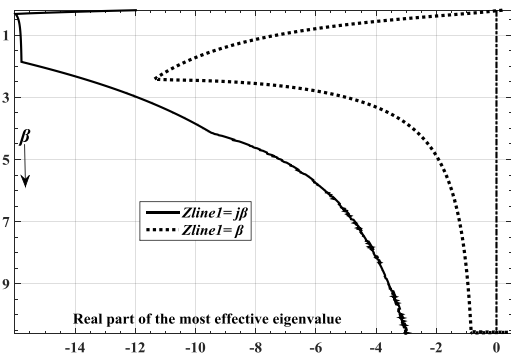


Fig. 14. Real part of the most effective eigenvalue as a function of  $r_{line1}$  and  $x_{line1}$  when DG3 is disconnected,  $m_p=[10\ 10]\times 1e-5$ .

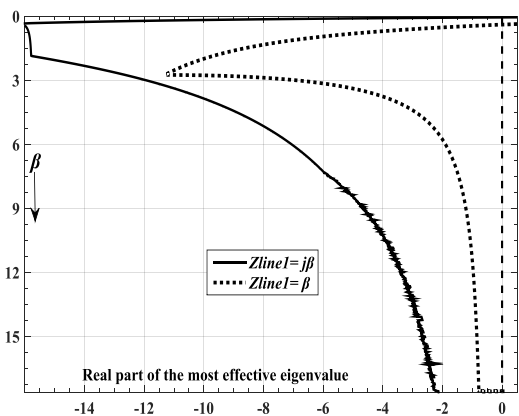


Fig. 15. Real part of the most effective eigenvalue as a function of  $r_{line1}$  and  $x_{line1}$  when DG3 is disconnected,  $m_p=[15\ 10]\times 1e-5$

The results of the reactance show a similar performance for all values except those very close to zero. The most effective eigenvalue continually moves toward unstable region as  $x_{line1}$  is increased. The system goes to an unstable state when  $x_{line1}$  is reached 48.4  $\Omega$  in the case of the same droop gains and 76.4  $\Omega$  for different droop gains which are about 5 times larger than those for  $r_{line1}$ . Using different droop gains make the power flow of Line 1 less so as Fig. 15 shows, the stability is attained in this case for larger values of the resistance and reactance.

It should be noted that it is impossible to obtain these figures and also Fig. 8 using the conventional small-signal methods due to that the steady-state operating point of the system changes when line impedances are increased. Calculation of a steady-state operating point for each value of line impedances is also impossible and takes very long time using Simulink. However, using the eigenvalue calculator makes it possible to perform such huge computations up to at most 84 ms as will be seen in Table 6.

**Simulation time comparison:** One of the main advantages of the proposed method is time-saving. Execution time and the maximum acceptable time-step of

the tests are given in Table 6 for the proposed method and Simulink. Using *Intel Pentium G2020 Processor* and 4GB of memory, the two methods were implemented within the MATLAB computing environment. The table shows that the proposed method gives the superior performance considering simulation time. The execution time of the proposed method is at least 17.5 times smaller than that of Simulink mostly due to that the maximum acceptable time-step of the proposed method can be selected at least 50 times greater than that of Simulink. It is worth mentioned that *variable-step* and *ode23tb* solver is selected for Simulink to boost its performance. This performance is especially significant when optimal issues such as energy management systems are dealt with [13].

Table 6 shows the number of iterations required to calculate eigenvalues using the eigenvalue calculator and the dynamic simulation for the steady-state or final values of eigenvalues. The error tolerances of the stopping criterions,  $\varepsilon_A$  and  $\varepsilon_X$ , are selected 0.001. To select T, the low-frequency modes of IBMGs must be considered. If  $T=0.1$  s, the stopping criterion of the dynamic simulation can check the magnitudes of oscillations even with a frequency of 5 Hz which ensures that the steady-state is reached completely. In Figs. 8, 14 and 15,  $\alpha$  and  $\beta$  are increased from 0.2 to 20 with incremental-step 0.2. The results show that the eigenvalue calculator needs at least (approximately) 25 times fewer iterations to obtain eigenvalues and as can be seen in Tables 3, 4 and 5, it gives the convincing results. This performance makes it possible to evaluate the system stability as a function of line impedances in Figs. 8, 14 and 15 as fast as given in Table 6. For these figures in table 10, the average numbers of the iterations are given which are larger than the others. As discussed, when line impedances increase, the stability becomes worse so the number of iterations increases due to high oscillations. However, even when the stability is very weak, the number of iterations is not more than 500 at most. Table 7 also shows that the inductive lines need more iterations than the resistive lines.

To calculate eigenvalues using conventional methods like [10], a steady-state operating point must be found by solving load-flow equations which must be linearized around that point in the next step. However, the proposed method without needing those complicated processes calculates the eigenvalues very quickly, as shown in Table 7. Therefore, the proposed method makes the system stability evaluation possible without performing time-consuming dynamic load-flow analysis using Simulink and other time-step simulations.

**TABLE 6. MAXIMUM ACCEPTABLE TIME-STEP AND EXECUTION TIME OF DIFFERENT TESTS**

Tests	Proposed method		Simulink	
	Time (s)	Time-step	Time (s)	Time-step
Test 1	3	1e-3	102	5e-6
Test 2	12	1e-4	212	2e-6
Test 3	5	5e-4	156	5e-6
Fig. 8	Different droop gains	8	1e-3	NA
	The same droop gains	25		
Fig. 14	R	24	1e-3	NA
	X	38		
Fig. 15	R	28	1e-3	NA
	X	84		

**TABLE 7. THE NUMBER OF ITERATIONS REQUIRED TO CALCULATE EIGENVALUES IN DIFFERENT TESTS**

Tests	Eigenvalue calculator		Steady-state or final values	
	The same droop gains	different droop gains	The same droop gains	different droop gains
Test 1	22	18	721	608
Test 2	84	49	5799	5649
Test 3	17	97	1578	2378
Fig. 8	42.5	13.2	NA	NA
Fig. 14 and 15 (average)	R	67	NA	NA
	X	112		

## 5- CONCLUSION

In this paper, modeling and analysis of islanded IBMGs were investigated using a new LTI state-space model. All dynamics of IBMGs except the switching action were considered in the model. To correct the linear model and perform a dynamic simulation, an iterative method was proposed. The analysis of the eigenvalues and stability of IBMGs is easy and fast using the proposed method due to those load-flow solutions to obtain the steady-state operating point of IBMGs are no longer needed and eigenvalues are derived directly. Eigenvalues were corrected dynamically when a fault occurred and they were also independent of the steady-state operating point which made the analysis of large disturbances as simple and fast as small-signal. The proposed method has also showed the superior performance considering the simulation time. The proposed LTI model has simplified stability assessment and analysis of large IBMGs due to linearity.

## REFERENCES

[1] R. H. Lasseter, Microgrids and Distributed Generation. Journal of Energy Engineering, 133 (2007), 144–149.  
[2] IEEE P1547 Standard for Distributed Resources Interconnected with Electric Power Systems, IEEE P1547 Std., Sep. 2002.

[3] F. Katiraei, M. R. Iravani, and P. W. Lehn, Microgrid Autonomous Operation During and Subsequent to Islanding Process, IEEE Trans. On Power Delivery, 20(2005) 248-257.  
[4] Gao, M., Chen, M., Jin Ch., Guerrero, J. M., Qian, Zh. M., 2013. Analysis, design, and experimental evaluation of power calculation in digital droop-controlled parallel microgrid inverters. Journal of Zhejiang University SCIENCE C, 14(1): 50-64.  
[5] B. Bahrani, H. Karimi, R. Iravani, Decentralized Control of Parallel Connection of Two Distributed Generation Units, Industrial Electronics, 2009. IECON '09. 35th Annual Conference of IEEE, 2009, 358-362.  
[6] N. Cai, J. Mitra, A multi-level control architecture for master-slave organized microgrids with power electronic interfaces, Electric Power Systems Research, 109 (2014), 8–19.  
[7] F. Gao and R. Iravani, “A Control Strategy for a Distributed Generation Unit in Grid-Connected and Autonomous Modes of Operation,” Power Delivery, IEEE Trans., vol. 23, no. 2, pp. 850–859, Apr 2008.  
[8] F. Katiraei, and M. R. Iravani, “Power Management Strategies for a Microgrid with Multiple Distributed Generation Units,” Power Systems IEEE Trans., vol. 21, no. 4, pp. 1821-1831, Nov. 2006.  
[9] Vandoorn T. L., Renders B., Degroote L., Meersman B., Vandeveldel L., “Active Load Control in Islanded Microgrids Based on the Grid Voltage” Smart Grid, IEEE Trans. Vol.2, no. 1, pp. 139-151, Mar. 2013.  
[10] N. Pogaku, M. Prodanovic, and T. C. Green, “Modeling, Analysis and Testing of Autonomous Operation of an Inverter-Based Microgrid,” Power Electronics IEEE Trans., vol. 22, no. 2, pp. 613–625, Mar. 2007.  
[11] N. Bottrell, M. Prodanovic, T. C. Green, “Dynamic Stability of a Microgrid with an Active Load” Power Electronics IEEE Trans., Vol. 28, no. 11, pp. 5107 – 5119, Nov. 2013.  
[12] H. Ch. Chiang, Chi-Yung Yen and K. T. Chang, “A frequency-dependent droop scheme for parallel control of ups inverters” Journal of the Chinese Institute of Engineers, Vol. 24, No. 6, pp. 699-708, 2001  
[13] E. Barklund, N. Pogaku, M. Prodanovic, C. Hernandez-Aramburo, and T. Green, “Energy Management in Autonomous Microgrid Using Stability-Constrained Droop Control of Inverters” Power Electronics, IEEE Trans., vol. 23, no. 5, pp. 2346–2352, Sept 2008.  
[14] Seidi Khorramabadi, S, Bakhshai, A, “Critic-Based Self-Tuning PI Structure for Active and Reactive

- Power Control of VSCs in Microgrid Systems” Smart Grid, IEEE Trans. Vol. 6, No. 1, pp. 92-103, Jan. 2015.
- [15] J. Vasquez, J. Guerrero, A. Luna, P. Rodriguez, and R. Teodorescu, “Adaptive Droop Control Applied to Voltage-Source Inverters Operating in Grid-Connected and Islanded Modes,” IEEE Trans. Industrial Electronics, vol. 56, no. 10, pp. 4088 – 4096, Oct 2009.
- [16] Bevrani, H., Shokoohi S., “An Intelligent Droop Control for Simultaneous Voltage and Frequency Regulation in Islanded Microgrids” Smart Grid, IEEE Trans. Vol. 4, No. 3, pp. 1505-1513, Sept. 2013.
- [17] Savaghebi, M., Jalilian, A., Vasquez, J.C., Guerrero, J. M., “Secondary Control Scheme for Voltage Unbalance Compensation in an Islanded Droop-Controlled Microgrid” Smart Grid, IEEE Trans. Vol. 3, No. 2, pp. 797-807, June 2012.
- [18] Laghari, J. A., Mokhlis, H., Karimi, M., Bakar, A. H. A., Hasmaini M., 2015. A new technique for islanding operation of distribution network connected with mini hydro. *Frontiers of Information Technology & Electronic Engineering*. 16(5):418-427.
- [19] J. Kim, J. Guerrero, P. Rodriguez, R. Teodorescu, and K. Nam, “Mode Adaptive Droop Control With Virtual Output Impedances for an Inverter-Based Flexible AC Microgrid,” *Power Electronics, IEEE Trans on*, vol. 26, no. 3, pp. 689 –701, Mar 2011.
- [20] M. Hua, H. Hu, Y. Xing, and J. Guerrero, “Multilayer Control for Inverters in Parallel Operation Without Intercommunications,” *IEEE Trans. Power Electronics*, vol. 27, no. 8, pp. 3651 – 3663, Aug 2012.
- [21] Z. Zeng, H. Yang, R. Zhao, Study on small signal stability of microgrids: A review and a new approach, *Renewable and Sustainable Energy Reviews*, 15 (2011) 4818–4828.
- [22] M. Marwali, J.-W. Jung, and A. Keyhani, Stability Analysis of Load Sharing Control for Distributed Generation Systems, *Energy Conversion, IEEE Trans.*, 22 (2007) 737–745.
- [23] S. Iyer, M. Belur, and M. Chandorkar, A Generalized Computational Method to Determine Stability of a Multi-inverter Microgrid, *Power Electronics, IEEE Trans.*, 25 (2010) 2420–2432.
- [24] N. Jayawarna, X. Wu, Y. Zhang, N. Jenkins, and M. Barnes, Stability of a Microgrid, *The 3rd IET International Conference on Power Electronics, Machines and Drives*, (2006) 316–320.
- [25] Johnson B.B., Davoudi A., Chapman P.L., Sauer P., Microgrid dynamics characterization using the automated state model generation algorithm, *Proceedings of 2010 IEEE International Symposium on Circuits and Systems (2010)* 2758 – 2761.
- [26] Chakraborty S., Simões M. G., Kramer, W. E., *Power Electronics for Renewable and Distributed Energy Systems: A Sourcebook of Topologies, Control and Integration*, Springer London, Green Energy and Technology (2013) 483-484.